García-Rodríguez, D.; Corral, JL.; Llorente, R. (2018). Design of asymmetrical directional couplers on ridge and strip SOI technology with high-dimensional variation tolerance. Optics Letters. 43(11):2491-2494. https://doi.org/10.1364/OL.43.002491

# Design of Asymmetrical Directional Couplers on Ridge and Strip SOI technology with high dimensional variation tolerance

**DAVID GARCIA-RODRIGUEZ,* JUAN L. CORRAL AND ROBERTO LLORENTE**

*Nanophotonics Technology Centre, Universitat Politècnica de València, Camino de Vera, s/n, 46022, Valencia, Spain*
**Corresponding author: dgarciarodriguez@ntc.upv.es*

Received XX Month XXXX; revised XX Month, XXXX; accepted XX Month XXXX; posted XX Month XXXX (Doc. ID XXXXX); published XX Month XXXX

**The supermode analysis of asymmetrical directional couplers (ADC) based on SOI technology for strip and ridge structures at 1550 nm is herein reported targeting to reduce ADC device fabrication requirements. The reported analysis based on supermodes permits to assess the sensitivity of the ADC coupling efficiency by calculating the index difference between even and odd supermodes. Optimum designs have been found for 100 nm and 400 nm gaps, respectively, capable of converting and (de) multiplexing both $TE_0$ and $TE_1$ modes taking into account the width, gap, height and slab thickness variations produced with respect to the nominal design. © 2018 Optical Society of America**

***OCIS codes:*** *(060.1810) Buffers, couplers, routers, switches, and multiplexers; (060.4230) Multiplexing; (130.3120) Integrated optics devices; (230.7400) Waveguides, slab.*

Data traffic demand is nowadays increasing dramatically due to the introduction of new telecommunication services like machine-to-machine communications in the internet-of-things (IoT) paradigm, and the continuous increase of video consumption in high bitrate-demanding formats as 4K [1]. Optical fiber capacity is increasing at approximately one order of magnitude per year [2]. If current growth rate continues, the commercial capacity may reach its upper limit within the next decade. In order to accommodate future data traffic growth, the space-dimension must be considered in the data multiplexing scheme [3].

Spatial-Division multiplexing (SDM), both in multicore-fiber [4], or in few-mode fibers supporting mode-division multiplexing (MDM), has been appointed as promising technique to avoid this capacity crunch [5-15]. Silicon on insulator (SOI) or planar lightwave circuit (PLC) processing technologies are optimal candidates to produce cost-effective optical devices for modal multiplexing in MDM transmission systems [8-17]. In such systems, mode (de)multiplexers are the key devices. Several mode (de)multiplexers based on Asymmetric Directional Couplers (ADCs) [8], Y junction [10] or in multimode interference (MMI) [13] have been reported in the literature.

These devices are typically fabricated in PLC technology, which offers several advantages such as low insertion loss, high yield rate and mass productivity; especially as the mode number increases [11,12]. However, higher sizes and long bending radii are usually required (exceeding 5 cm in some cases [14]). However, SOI technology offers a reduced size and shorter bending radii, which clearly improve the capability to integrate several functions [15].

ADC devices based on SOI technology with strip structure offer an excellent performance as mode (de)multiplexer but they require a precise phase-matching of the different optical modes and therefore they are inherently sensitive to fabrication errors [8,9,15]. In order to ease tolerances in the fabrication process, the analysis of the effective refractive indexes of the even and odd supermodes have been recently used to study the performance and the structure of different integrated devices based on coupling waveguides [16,17]. This method has been used to analyze the tolerance against variations in width, height and gap for strip and ridge directional couplers (DC), demonstrating that the DC ridge design is 4 times more robust [17].

This letter address the design of an ADC in SOI technology to convert between $TE_0$ and $TE_1$ modes with the objective of maximizing the tolerance against dimensional variations due to the fabrication process. The ADC coupling efficiency is expressed in terms of the effective index difference between even and odd supermodes and an analysis of the sensitivity of the coupling efficiency to variations on the width, height, gap or etching depth dimensions has been carried out for both strip and ridge ADCs. Design guidelines to maximize the device tolerance are given and the best design is selected.

## Asymmetrical Directional Coupler model

Figure 1 depicts the scheme of a MDM link. At the transmitter, two directly modulated lasers emit at 1550 nm propagating the $LP_{01}$ modes in their respective single-mode fibers (SMFs). One $LP_{01}$

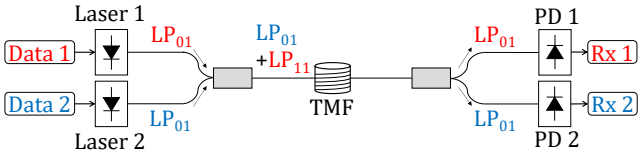


Fig. 1. Scheme for mode-division multiplexing (MDM) at 1550 nm with two-mode fiber (TMF) optical transmission media.

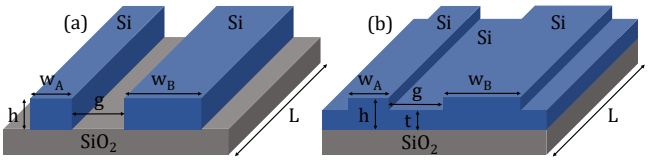


Fig. 2. Mode converter and (de)multiplexer based on SOI technology for two structure types. (a) Strip and (b) ridge.

mode must be converted to a higher mode ($LP_{11}$) and multiplexed with the other $LP_{01}$ mode. In our case, an ADC based on SOI technology has been selected as mode converter and multiplexer. Both $LP_{01}$ modes will be coupled to the SOI ADC through input grating couplers converting the signals to $TE_0$ modes. One of the $TE_0$ modes (corresponding to the upper branch in Fig. 1) will be converted to the $TE_1$ and multiplexed to a common waveguide. Finally, both modes will be coupled to the two-mode fiber (TMF) through an output grating coupler, propagating now the $LP_{01}$ and $LP_{11}$ modes. At the receiver side, the same ADC is used to demultiplex each mode to the corresponding photodiode.

We propose two different designs, strip and ridge, for the ADC, as is depicted in Fig. 2. In both cases, the waveguide widths are not equal and the device operation depends on achieving the phase-matching condition, where the effective index of the $TE_0$ mode in the waveguide A ($w_A$) must match the effective index of the $TE_1$ mode in the waveguide B ($w_B$). Besides the waveguide widths, the main parameters used in the device optimization are the gap between waveguides, $g$, the coupling length, $L$, the height, $h$, and the slab thickness, $t$ ($t$=0 for the strip structure).

Considering that the power is launched only into mode $a$ at z=0 (initial conditions $A(0)\neq 0$ and $B(0)=0$), the mode expansion coefficients in the two coupled waveguides ($A(z)$ mode $a$ in waveguide A and $B(z)$ mode $b$ in waveguide B) as a function of the propagation distance are given by [18]

$$\tilde{A}(z) = \tilde{A}(0)\left(cos(\beta_c z) - \frac{i\delta}{\beta_c} sin(\beta_c z)\right) e^{i\delta z} \quad \textbf{(1)}$$

$$\tilde{B}(z) = \tilde{A}(0)\left(\frac{i\kappa_{ba}}{\beta_c} sin(\beta_c z)\right) e^{-i\delta z} \quad \textbf{(2)}$$

$$A(z) = \tilde{A}(z) e^{i\kappa_{aa} z} \quad \textbf{(3)}$$

$$B(z) = \tilde{B}(z) e^{i\kappa_{bb} z} \quad \textbf{(4)}$$

where $\kappa_{aa}$ and $\kappa_{bb}$ are the self-coupling coefficients that take into account the variation in the propagation constant of each mode due to the perturbation caused by the other waveguide, $\kappa_{ab}$ and $\kappa_{ba}$ are the mutual coupling coefficients between both modes which depend on the waveguide separation, $g$. Finally, $\beta_c$ and $\delta$, the phase mismatch, can be expressed as

$$2\delta = (\beta_b + \kappa_{bb}) - (\beta_a + \kappa_{aa}) \quad \textbf{(5)}$$

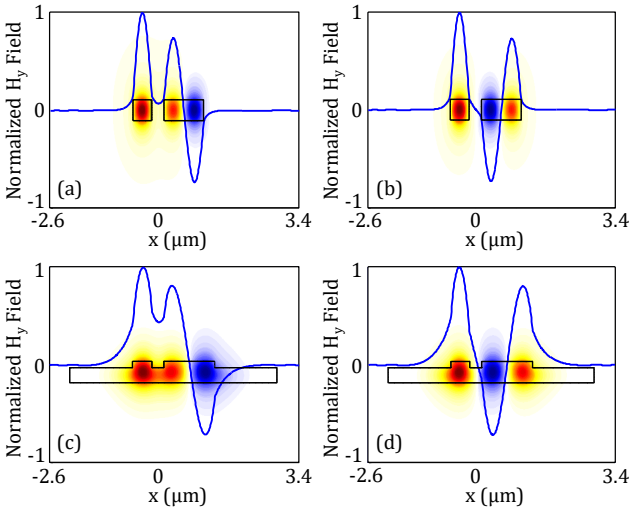


Fig. 3. Normalized $H_y$ field of even and odd supermodes in the ADC for $TE_0$ and $TE_1$ modes. (a) Even and (b) odd supermodes in strip structure (c) Even and (d) odd supermodes in ridge structure.

$$\beta_c = \sqrt{\kappa_{ab}\kappa_{ba} + \delta} \quad \textbf{(6)}$$

where $\beta_a$ and $\beta_b$ are the propagation constants of modes $a$ and $b$ at their respective unperturbed waveguides. The complete field profile across the directional coupler can be obtained as a combination of the two mode fields as

$$\boldsymbol{E}(r) = \tilde{A}(0)\left(\mathcal{E}_1(x,y)e^{i\beta_1 z} + \mathcal{E}_2(x,y)e^{i\beta_2 z}\right) \quad \textbf{(7)}$$

taking into account that

$$\mathcal{E}_1(x,y) = \frac{(\beta_c-\delta)\hat{\mathcal{E}}_a(x,y)+\kappa_{ba}\hat{\mathcal{E}}_b(x,y)}{2\beta_c} \quad \textbf{(8)}$$

$$\mathcal{E}_2(x,y) = \frac{(\beta_c+\delta)\hat{\mathcal{E}}_a(x,y)-\kappa_{ba}\hat{\mathcal{E}}_b(x,y)}{2\beta_c} \quad \textbf{(9)}$$

where $\hat{\boldsymbol{\mathcal{E}}}_{\boldsymbol{a}}(x,y)$ and $\hat{\boldsymbol{\mathcal{E}}}_{\boldsymbol{b}}(x,y)$ are the normalized mode profiles of both modes in their respective isolated waveguides and

$$\beta_1 = \bar{\beta} + \beta_c \quad \textbf{(10)}$$

$$\beta_2 = \bar{\beta} - \beta_c \quad \textbf{(11)}$$

$$2\bar{\beta} = (\beta_b + \kappa_{bb}) + (\beta_a + \kappa_{aa}) \quad \textbf{(12)}$$

The total field in the coupler is a linear combination of two independent patterns $\boldsymbol{\mathcal{E}}_1(x,y)$ and $\boldsymbol{\mathcal{E}}_2(x,y)$ propagating with different propagation constants $\beta_1$ and $\beta_2$. These modes of the two-waveguide structure of the directional coupler are known as the supermodes of the structure and an example of their profile are shown in Fig. 3 for both strip and ridge structures. In this figure, the magnitude of the field profile of the even and odd supermodes in the center of the guides ($y$=0) along the x-direction are shown with a blue solid line. The main characteristics of the supermodes depend on $\delta$, $\kappa_{ab}$ and $\kappa_{ba}$.

From Eq. (2) the coupling efficiency from waveguide A to waveguide B in the ADC can be expressed as

$$K = \frac{|\kappa_{ba}|^2}{\beta_c^2} \sin^2\left(\frac{\pi \Delta n}{\lambda} L\right) \quad \textbf{(13)}$$

where $\Delta n$ is the effective index difference between the even and odd supermodes; $\lambda$ is the wavelength; and $L$ is the length of the coupler.

If the modes to be coupled are phase-matched, then $\delta=0$ and $\kappa_{ab} = \kappa_{ba}^*$ and the coupling efficiency is maximized,

$$K = \sin^2\left(\frac{\pi \Delta n}{\lambda} L\right) \quad \textbf{(14)}$$

In this case, if we consider $\alpha$ as an arbitrary geometric parameter (i.e., $\alpha$ can be replaced by $w$, $g$, $h$, or $t$), for the minimum coupling length, $L$, in order to achieve $K=1$, the sensitivity of the coupling efficiency to this parameter can be expressed as [17]

$$\frac{\partial K}{\partial \alpha} = 2\sin^{-1}\left(\sqrt{K}\right)\sqrt{K(1-K)}\frac{1}{\Delta n}\frac{\partial \Delta n}{\partial \alpha} \quad \textbf{(15)}$$

## Sensitivity analysis

The sensitivity of the coupling efficiency is directly determined by the sensitivity parameter $(\partial \Delta n/\partial \alpha)/\Delta n$. A robust ADC design should consider the fabrication tolerances in the different device dimensions in order to optimize the fabrication process yield.

The common material used in the investigation of several integrated applications is the silicon-on-insulator wafer with a 220 nm silicon thickness [19]. The refractive indices of Si and $SiO_2$ at 1550 nm are $n_{Si}$= 3.4764 and $n_{SiO2}$=1.4440, respectively, and the eigenmodes' effective indexes in the waveguides will be calculated with the three-dimensional (3D) beam propagation method (3D-BPM). For this height, the TE polarization is usually preferred for its lower bending losses [19].

Two structure types will be considered in the ADC coupler design, strip and ridge. In the strip structure a typical width for a single-mode waveguide is $w_A$=450 nm with an effective index value of $n_{eff\_TE0}$=2.4111 at the wavelength design, 1550 nm. The width of the two-mode waveguide must be selected to obtain a similar value for the effective index of the $TE_1$ mode ($w_B$=962 nm for an unperturbed waveguide) so the phase-matched condition is fulfilled. The effective index value for the ridge ($t$=150 nm) single-mode waveguide is $n_{eff\_TE0}$=2.6689 when $w_A$=450 nm and the corresponding width for the two-mode waveguide should be $w_B$=1227 nm if an isolated waveguide is considered.

Supermodes permit to analyze the sensitivity of the ADC coupling efficiency by calculating the $\Delta n$ between the even and odd supermodes. The effective indexes of the even and odd supermodes have been also calculated with the 3D-BPM method.

Different designs have been considered ($w_A$ from 430 nm to 470 nm and $g$=100 nm, 200 nm, 300 nm and 400 nm (only for the ridge design)) and for each case the two-mode width, $w_B$, has been selected in order to fulfill the phase-matched condition, $\delta=0$, when the influence of both waveguides are taken into account (Eq. (5)). Small variations of all parameters ($w$, $g$, $h$ and $t$) have been introduced in the simulations in order to analyze the robustness of the ADC against fabrication tolerances.

If the waveguide width is increased, the modes would be more confined in the center of the waveguide, which would reduce $\Delta n$. However, $\Delta n$ is also dependent on the gap between waveguides; therefore, a decrease in the gap, $g$, increases the mode overlap between the two waveguides and consequently $\Delta n$. If the variations in the waveguide widths are perfectly anti-correlated with the gap variations, that is to say, the width variations are supposed to be symmetric with respect to their centerlines, a robust coupler design must fulfilled

$$\frac{\partial \Delta n}{\partial w} - \frac{\partial \Delta n}{\partial g} \approx 0 \quad \textbf{(16)}$$

expression that was used also in [17] to select the most tolerant dimensions of symmetric DC and where a significant anti-correlation between width and gaps variations was found in the device fabrication (correlation coefficient, $\rho$=-0.6).

Figure 4 depicts the simulated sensitivity parameter for the width, gap and height variations in the strip structure at 1550nm. From Fig. 4(a) it can be stated that in terms of sensitivity to width variations the 100 nm gap offers a more robust design than the configurations with a wider gap (200 nm and 300 nm). In fact, for the nominal design ($w_A$=450 nm and $w_B$=969 nm), the 100 nm gap obtains a value of $-0.64\cdot10^{-2}$nm$^{-1}$. However, the 200 nm and 300 nm gaps obtained worse values ($-1.2\cdot10^{-2}$ nm$^{-1}$ and $-3.3\cdot10^{-2}$ nm$^{-1}$, respectively) for $w_A$=450 nm, being 2 and 5 times less robust than the 100 nm gap. If we consider the whole simulated $w_A$ width range (430 nm to 470 nm), the sensitivity to variations in the waveguides width remains practically constant for a fixed gap value. However, in terms of sensitivity to the gap dimension (Fig. 4(b)), the sensitivity worsens slightly when the width increases. The difference between all gaps is quite small obtaining the best response for the 300 nm gap, as can be seen in Fig. 4(b). We have not considered smaller gaps than 100 nm due to the additional difficulty in the fabrication process and the increase of the $TE_0$ coupling to the TMF, which may result in a higher crosstalk level (-23.4 dB at 1550 nm for g=100 nm [8]).

In Fig. 4(c), the simultaneous anti-correlated variations in the width and gap parameters for the purpose of fulfilling Eq. (16) remark that the 100 nm gap achieves the optimum result with a value of $-0.074\cdot10^{-2}$ nm$^{-1}$ for $w_A$=450 nm. However, the 200 nm and 300 nm gaps obtain a value of $-0.66\cdot10^{-2}$ nm$^{-1}$ and $-2.8\cdot10^{-2}$ nm$^{-1}$ being 9 and 38 times less robust than the 100 nm gap. As it happened with the widths variations, the sensitivity to anti-correlated variations in width and gap dimensions remain almost constant when a design with different $w_A$ is considered (±20 nm respect to $w_A$=450 nm). Therefore, the

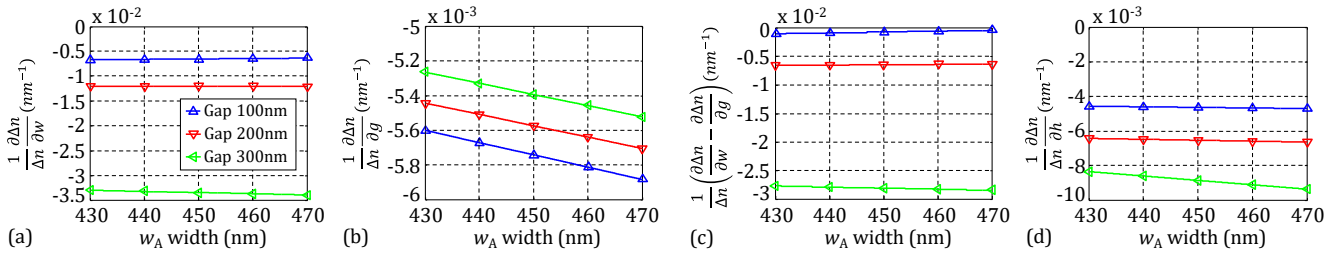


Fig. 4. Fractional change in $\Delta n$ for strip structure with respect to (a) waveguide width, $w$, (b) waveguide gap, $g$, (c) correlated changes in $w$ and $g$, and (d) waveguide height, $h$.

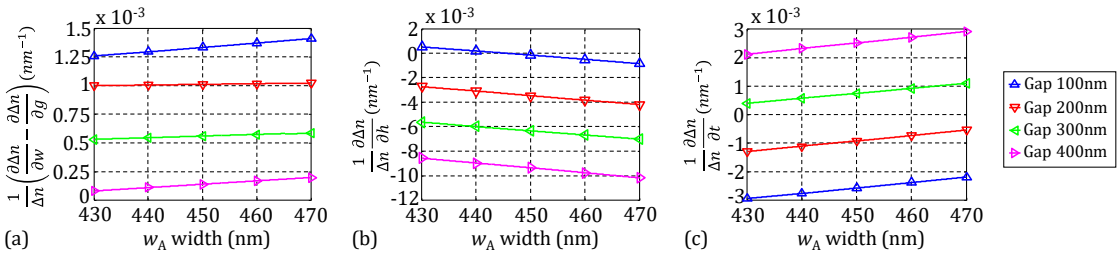


Fig. 5. Fractional change in $\Delta n$ for ridge structure with respect to (a) correlated changes in $w$ and $g$, (b) waveguide height, $h$ and (c) slab thickness, $t$.

selection of the $w_A$ parameter is not critical. In Fig. 4(d) the sensitivity to height variations is depicted and the best response is again achieved for the 100 nm gap. The magnitude order of the sensitivity parameter is in the range of $10^{-3}$ nm$^{-1}$ (as it happens with gap variations), whilst it is an order of magnitude higher in the case of the width and gap variations. Consequently, more attention must be paid to the width and gap dimension tolerances during the design process.

The ADC with ridge structure was simulated considering the same parameters that were used in the strip simulations, but now including a new parameter, the slab thickness, $t$. In Fig. 5(a), the sensitivity to the anti-correlated width and gap variations is shown. The best response was obtained for the highest gap (400 nm) with a value of $0.14{\cdot}10^{-3}$ nm$^{-1}$ ($w_A$=450 nm and $w_B$=1223 nm). For the rest of gaps, the different values were $0.55{\cdot}10^{-3}$ nm$^{-1}$, $1{\cdot}10^{-3}$ nm$^{-1}$ and $1.3{\cdot}10^{-3}$ nm$^{-1}$ being 4, 7 and 10 times less robust than the 400 nm gap, respectively. If we consider a range of ±20 nm around the nominal design widths, the sensitivity parameter of all gaps remain practically constant with small variations. The difference between all gaps has significantly decreased in comparison with the strip structure. However, as shown in Fig. 5(b), the sensitivity to height variation presents the opposite behavior and the smallest gap (100 nm) has the best sensitivity parameter with a value of $-0.1{\cdot}10^{-3}$ nm$^{-1}$ in the nominal design. In both SOI structures (strip and ridge) the optimum result is achieved for the minimum gap.

In Fig. 5(c), the simulated sensitivity parameter for the slab thickness variation is shown. The optimum gap is achieved between two different gaps (200 nm and 300 nm) depending on the $w_A$ width. When the nominal design is considered, the optimum gap is 300 nm with a value of $0.7{\cdot}10^{-3}$ nm$^{-1}$ unlike the 200 nm gap that obtained a value of $-0.9{\cdot}10^{-3}$ nm$^{-1}$. For $w_A$ widths lower than 450 nm is better to choose the 300 nm gap whilst for broader widths, it is better to select the 200 nm gap.

From the results obtained in Fig. 5, it can be stated that the optimum gap is the 400 nm considering the anti-correlated changes in width and gap, the 100 nm gap for changes in height and 300 nm (when $w_A$ is 450 nm) for changes in the slab thickness. However, in SOI fabrication process, the most critical parameter is the width and gap variation [20], therefore, the optimum ridge design is achieved when the 400 nm gap is selected. According to the trend shown in Fig. 5(a), a 500 nm gap would obtain similar values of the sensitivity parameter module against $w$ and $g$ variations but offering a lesser compact design. Furthermore, the sensitivity will be worst against $h$ and $t$ variations following the trend shown in Fig. 5(b) and Fig. 5(c).

The proposed designs (100 nm gap for the strip structure and 400 nm gap for the ridge structure) for the ADCs are optimum in order to convert and (de)multiplex the $TE_0$ mode into the $TE_1$ mode taking into account the width and gap variations produced in the nominal design due to the fabrication tolerances. However, the ridge structure is more tolerant than the strip structure by a factor of 6 ($0.14{\cdot}10^{-3}$ nm$^{-1}$ by $-0.074{\cdot}10^{-2}$ nm$^{-1}$, respectively), a similar performance as the obtained for the symmetric directional couplers [17].

**Funding.** Ministerio de Economía y Competitividad (MINECO) (TEC2015-70858-C2-1-R, RTC-2014-2232-3).

## References

1. "Cisco Visual Networking Index: Forecast and Methodology, 2016–2021," Cisco White Paper, https://goo.gl/DXQUFE
2. R.-J. Essiambre, G. Kramer, P. J. Winzer, G. J. Foschini, and B. Goebel, J. Lightwave Technol. **28**, 662 (2010).
3. D. J. Richardson, Philos. Trans. R. Soc. A **374**, 20140441 (2016).
4. T. Mizuno, H. Takara, A. Sano, and Y. Miyamoto, J. Lightwave Technol. **34**, 582 (2016).
5. P. J. Winzer, Nat. Photonics **8**, 345 (2014).
6. D. Melati, A. Alippi, A. Annoni, N. Peserico, and A. Melloni, Opt. Lett. **42**, 342 (2017).
7. D. Garcia-Rodriguez, J. L. Corral, and R. Llorente, IEEE Photon. Technol. Lett. **29**, 929 (2017).
8. D. Garcia-Rodriguez, J. L. Corral, A. Griol, and R. Llorente, Opt. Lett. **42**, 1221 (2017).
9. Y.-S. Lee, Z. Wang, Z.-Y. Li, Y. Li, Q. Li, C. Cui, and C.-Q. Wu, Opt. Commun. **406**, 173 (2018).
10. C. Sun, Y. Yu, M. Ye, G. Chen, and X. Zhang, Sci. Rep. **6**, 38494 (2016).
11. N. Hanzawa, K. Saitoh, T. Sakamoto, T. Matsui, K. Tsujikawa, T. Uematsu, and F. Yamamoto, J. Lightwave Technol. **33**, 1161 (2015).
12. Y. Yamashita, T. Fujisawa, S. Makino, N. Hanzasa, T. Sakamoto, T. Matsui, K. Tsujikawa, F. Yamamoto, K. Nakajima, and K. Saitoh, J. Lightwave Technol. **35**, 2252 (2017).
13. A. Zanzi, A. Brimont, A. Griol, P. Sanchis, and J. Marti, Opt. Lett. **41**, 227 (2016).
14. N. Hanzawa, K. Saitoh, T. Sakamoto, T. Matsui, K. Tsujikawa, M. Koshiba, and F. Yamamoto, Opt. Express **22**, 29321 (2014).
15. J. Wang, S. He, and D. Dai, Laser Photon. Rev. **8**, L18 (2014).
16. C. Pan and B. M. A. Rahman, J. Lightwave Technol. **34**, 2288 (2016).
17. J. C. Mikkelsen, W. D. Sacher, and J. K. S. Poon, Opt. Express **22**, 3145 (2014).
18. J. M. Liu, Photonic Devices (Cambridge University, 2007).
19. D. X. Xu, J. H. Schmid, G. T. Reed, G. Z. Mashanovich, D. J. Thomson, M. Nedeljkovic, X. Chen, D. Van Thourhout, S. Keyvaninia, and S. K. Selvaraja, IEEE J. Sel. Top. Quantum Electron. **20**, 422 (2014).
20. J. L. Corral, D. Garcia-Rodriguez, and R. Llorente, IEEE Photon. Technol. Lett. **28**, 425 (2016).

## References


1. Cisco. “Cisco Visual Networking Index: Forecast and Methodology, 2016–2021,” Cisco White Paper, Jun. 2017.
2. R. J. Essiambre, "Capacity Limit of Optical Fiber Networks", J. Lightwave Tech., vol. 28, no. 4, pp. 662-701, Feb. 2010.
3. D. J. Richardson, “New optical fibres for high-capacity optical communications subject areas,” Philos. Trans. Roy. Soc. A, vol. 374, 2016, Art.ID. 20140441.
4. T. Mizuno, H. Takara, A. Sano, and Y. Miyamoto, “Dense space-division multiplexing transmission systems using multi-core and multi-mode fiber,” J. Lightwave Technol. 34(2), 582–592 (2016).
5. P. J. Winzer, “Making spatial multiplexing a reality,” Nature Photon., vol. 8, pp. 345–348, 2014.
6. D. Melati et al., “Integrated all-optical MIMO demultiplexer for mode and wavelength-division-multiplexed transmission,” Opt. Lett., vol. 42, no. 2, pp. 342–345, 2017.
7. D. Garcia-Rodriguez et al. “Mode Conversion for Mode Division Multiplexing at 850 nm in Standard SMF”, IEEE Photon. Technol. Lett. 29(11), pp.929-932, Jun. 2017.
8. D. Garcia-Rodriguez et al., “Dimensional variation tolerant mode converter/ multiplexer fabricated in SOI technology for two-mode transmission at 1550 nm,” Opt. Lett. 42, pp. 1221-1224 Apr 2017.
9. Y. Le et al., “Three-mode all-optical (de)multiplexing on a SOI chip,” Opt. Commun., vol. 406, pp. 173–176, 2018.
10. C. Sun et al., “An ultra-low crosstalk and broadband two-mode (de) multiplexer based on adiabatic couplers,” Sci. Rep., 6 (2016).
11. N. Hanzawa et al., “PLC-based four-mode multi/demultiplexer with $lp_{11}$ mode rotator on one chip,” J. Lightwave Technol., vol. 33, no. 6, pp. 1161-2169, Mar. 2015.
12. Y. Yamashita et al., "Design and fabrication of broadband PLC-based two-mode multi/demultiplexer using a wavefront matching method", J. Lightw. Technol., vol. 35, no. 11, pp. 2252-2258, Jun. 2017.
13. A. Zanzi, "Compact and low-loss asymmetrical multimode interference splitter for power monitoring applications", Opt. Lett., vol. 41, no. 2, pp. 227-228, Jan. 2016.
14. N. Hanzawa et al., “Mode multi/demultiplexing with parallel waveguide for mode division multiplexed transmission,” *Opt. Exp.*, vol. 22, no. 24, pp. 29321–29330, 2014.
15. J. Wang, S. He, and D. Dai, “On-chip silicon 8-channel hybrid (de)multiplexer enabling simultaneous mode- and polarization-division multiplexing,” Laser Photon. Rev., vol. 8, no. 2, pp. L18–L22, Mar. 2014.
16. C. Pan et al., “Accurate Analysis of the Mode (de)multiplexer Using Asymmetric Directional Coupler,” J. Lightw. Technol., vol. 34, no. 9, pp. 2288–2296, May 2016.
17. J. C. Mikkelsen *et al.*, “Dimensional variation tolerant silicon-on-insulator directional couplers,” *Opt. Exp.*, vol. 22, no. 3, pp. 3145–3150, 2014.
18. M. Liu, Photonic Devices (Cambridge University, 2007).
19. D. X. Xu, J. H. Schmid, G. T. Reed, G. Z. Mashanovich, D. J. Thomson, M. Nedeljkovic, X. Chen, D. Van Thourhout, S. Keyvaninia, and S. K. Selvaraja, IEEE J. Sel. Top. Quantum Electron. 20, 422 (2014).
20. J.L Corral, D. Garcia-Rodriguez and R. Llorente, “Mode-selective couplers for Two-Mode Transmission at 850 nm in Standard SMF,” IEEE Photon. Technol. Lett., vol. 28, no. 4, pp. 425-428, Feb. 15, 2016.